Title

Nonlinear vibration of orthotropic rectangular membrane structures including modal coupling

Journal

Journal of Applied Mechanics, 85(6)

ISSN

0021-8936

Authors

Li, Dong
Zheng, Zhoulian
Todd, Michael

Publication Date

2018-06-01

DOI

10.1115/1.4039620

Peer reviewed

Nonlinear vibration of orthotropic rectangular membrane structures including modal coupling

Dong Li

School of Civil Engineering,
University of Chongqing,
83 Shabei Street,
Chongqing 400045, China;
Department of Structural Engineering,
University of California San Diego,
9500 Gilman Drive 0085,
La Jolla, CA 92093-0085
email: 20151601001@cqu.edu.cn

Zhou Lian Zheng

School of Civil Engineering,
University of Chongqing,
83 Shabei Street,
Chongqing 400045, China;
Chongqing Jianzhu College,
Chongqing 400072, China
email: zhengzl@cqu.edu.cn

Michael D. Todd[1]

Department of Structural Engineering,
University of California San Diego,
9500 Gilman Drive 0085,
La Jolla, CA 92093-0085
e-mail: mdtodd@ucsd.edu

[1] Corresponding author, mdtodd@ucsd.edu

Abstract

The membrane structure has been applied throughout different fields such as civil engineering, biology, and aeronautics, among others. In many applications, large deflections negate linearizing assumptions, and linear modes begin to interact due to the nonlinearity. This paper considers the coupling effect between vibration modes and develops the theoretical analysis of the free vibration problem for orthotropic rectangular membrane structures. Von Kármán theory is applied to model the nonlinear dynamics of these membrane structures with sufficiently large deformation. The transverse displacement fields are expanded with both symmetric and asymmetric modes, and the stress function form is built with these coupled modes. Then, a reduced model with a set of coupled equations may be obtained by the Galerkin technique, which is then solved numerically by the fourth-order Runge-Kutta method. The model is validated by means of an experimental study. The proposed model can be used to quantitatively predict the softening behavior of amplitude-frequency, confirm the asymmetric characters of mode space distribution, and reveal the influence of various geometric and material parameters on the nonlinear dynamics.

1 Introduction

Applications utilizing membrane structures are prevalent, ranging from traditional areas in mechanical engineering, civil engineering, space and aeronautics, etc. [1,2] to more modern areas such as robotics, biological devices, and musical instruments [3,4]. This is mainly because this type of structure is both relatively lightweight and highly flexible, which are often requirements for this diverse range of applications. However, these desirable properties often come at the expense of reduced stiffness. Consequently, they are prone to vibration, often with large deformations (several times the order of the thickness) that linear models cannot predict. This vibration may lead to reduced performance or even failure of the membrane structure.

Consequently, the vibration of membrane structures has attracted the attention of

researchers, and several relevant studies may be found. Kang and Lee [5] proposed an analytical expansion basis with sinusoidal functions to obtain the natural frequencies and mode shapes of rectangular membranes. Houmat [6] applied the h-p version of the finite element method to obtain the numerical results for natural frequencies for triangular and L-shaped membranes; shifted Legendre orthogonal polynomials were used during calculation procedure. Wu et al. [7] combined the differential quadrature (DQ) method with radial basis functions (RBFs) to analyze the free vibration of arbitrarily shaped membranes. The derivative at the reference point in a region was approximated as a linear weighted sum of functions before discretizing the Helmholtz equation for vibration. This idea was also applied by Amore [8], and a set of localized functions called "little sinc functions" were used to discretize the membrane regions. Noga [9] presented the complete derivation of governing equations for free transverse vibration of a compound double-membrane system. To solve the governing equation, the Bernoulli-Fourier method using the sinc function was used. Soares and Goncalves [10] considered both the linear and nonlinear vibration analysis pre-tensioned rectangular membranes. The mode shapes obtained from linear vibration analysis were used to approximate the nonlinear deformation field via a Galerkin method. Zheng et al. [11] derived the undamped governing vibration equations of orthotropic membranes and solved them with only symmetric mode functions; the hardening feature of the frequency response was obtained and discussed in detail. Liu et al. [12] subsequently extended that study to include viscous damping. Using symmetric mode functions, they obtained the asymptotic analytical solutions for frequency and displacement. Liu et al. [13] further developed this analysis into a nondestructive tool to monitor pretension in the membrane. In that applied development, in order to obtain a simple and rapidly convergent solution, only a single-term shape function was used. To validate these theoretical results, Guo et al. [14] designed an experiment and tested the dynamic characteristics. Zheng et al. [15] considered uncertainty in

the load and studied the stochastic vibration response. Furthermore, this random model with viscous damping was validated by experiment. Li et al. [16] analyzed the free vibration problem of rectangular membrane structures by means of a Galerkin method using symmetric modes. Laura et al. [17] applied Rayleigh Ritz and differential quadrature method to study circular and annular membrane axisymmetric modes.

Based on the literature summarized above, most of the recent studies neglect modal coupling, using only symmetric mode function expansions or a linearized theory. However, the effect of modal coupling between symmetric and asymmetric modes on nonlinear vibration behavior becomes more significant when strong nonlinear vibration is occurring; for example, after expanding the mode functions by symmetric and asymmetric modes, a softening nature of response can appear (e.g., see Refs. [18,19]), unlike the traditional hardening characteristics. Thus, this paper considers both symmetric and asymmetric mode functions to study the free vibration of membrane structures with this modal coupling effect and validate the analysis with experimental data.

This paper initially reviews the governing equations of the nonlinear free vibration of membrane structures, including von Kármán geometric nonlinearities. In order to model and analyze the coupling effect, the transverse deformation and stress are expressed in terms of finite sums of symmetric and asymmetric mode functions. Then, the infinite model may be transformed into a reduced-order modal model via the Galerkin technique. Finally, the nonlinear characteristics related to free vibrations may be found using Runge-Kutta numerical integration to solve the coupled modal equations. Furthermore, and very importantly, the reduced-order modal model is validated by experimental study. The effects of variables including pretension, material property, aspect ratio, and others on nonlinear characters are discussed in detail.

2 Nonlinear Mechanics Model and Numerical Solution

2.1 Model Development. A rectangular membrane structure model with length a, width b, and thickness h is shown in Fig. 1. N_{0x} and N_{0y} are the initial tensions along axis x and y, respectively. It should be noted that the membrane material is orthotropic. Its two orthogonal directions are the two principal fiber directions along axis x and y, respectively.

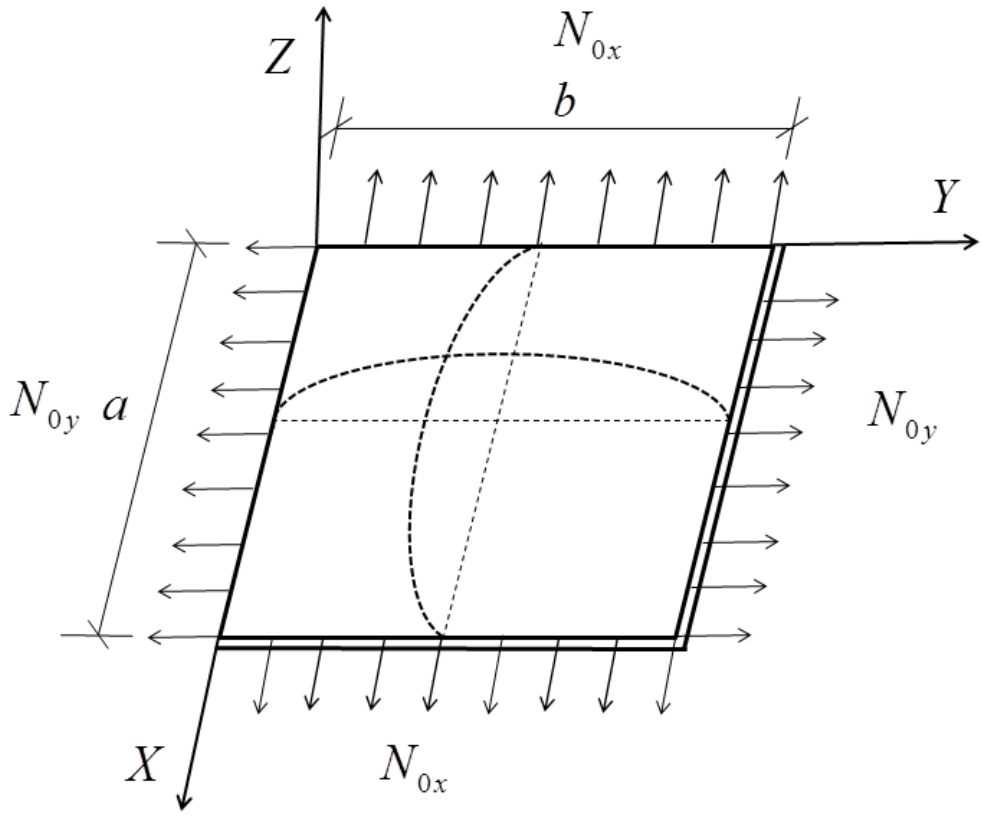

Fig. 1 Model of rectangular orthotropic membrane structure with pre-tension.

Since large deformation may cause the median surface to stretch, von Kármán geometric nonlinearity is included. The von Kármán nonlinear strain-displacement relations, to second order, are

$$\begin{cases} \varepsilon_x = \dfrac{\partial u}{\partial x} + \dfrac{1}{2}\left(\dfrac{\partial w}{\partial x}\right)^2 \\ \varepsilon_y = \dfrac{\partial v}{\partial y} + \dfrac{1}{2}\left(\dfrac{\partial w}{\partial y}\right)^2 \\ \gamma_{xy} = \dfrac{\partial v}{\partial x} + \dfrac{\partial u}{\partial y} + \dfrac{\partial w}{\partial x}\dfrac{\partial w}{\partial y} \end{cases}, \tag{1}$$

where ε_x and ε_y denote the axial strain along x and y axes, respectively, γ_{xy} denotes the shear strain, and u, v and w denote the displacements along *x, y*, and *z* axes, respectively. Based on Eq. (1), a compatibility equation that eliminates u and v may be derived as

$$\frac{\partial^2 \varepsilon_x}{\partial y^2} + \frac{\partial^2 \varepsilon_y}{\partial x^2} - \frac{\partial^2 \gamma_{xy}}{\partial x \partial y} = \left(\frac{\partial^2 w}{\partial x \partial y}\right)^2 - \frac{\partial^2 w}{\partial x^2}\frac{\partial^2 w}{\partial y^2}\ . \tag{2}$$

In the case of orthotropic material, the stresses are related to the strains by

$$\begin{cases} \varepsilon_x = \dfrac{1}{E_1}\sigma_x - \dfrac{\upsilon_2}{E_2}\sigma_y \\ \varepsilon_y = -\dfrac{\upsilon_1}{E_1}\sigma_x + \dfrac{1}{E_2}\sigma_y \\ \gamma_{xy} = \dfrac{\tau_{xy}}{G} \end{cases}, \tag{3}$$

where σ_x and σ_y denote the axial stress along x and y axes, respectively, τ_{xy} denotes the shear stress, E_1 and E_2 denote Young's modulus along x and y axes, respectively, G denotes the shear modulus, and υ_1 and υ_2 denote Poisson's ratio in x and y axes, respectively. The orthotropic material relation between Young's modulus and Poisson's ratio is

$$\frac{\upsilon_1}{E_1} = \frac{\upsilon_2}{E_2}. \tag{4}$$

Substituting the material model equations Eqs. (3)-(4) into the compatibility equation Eq. (2) yields

$$\frac{1}{E_1 h}\frac{\partial^2 N_x}{\partial y^2} - \frac{\upsilon_1}{E_1 h}\frac{\partial^2 N_x}{\partial x^2} + \frac{1}{E_2 h}\frac{\partial^2 N_y}{\partial x^2} - \frac{\upsilon_2}{E_2 h}\frac{\partial^2 N_y}{\partial y^2} - \frac{1}{Gh}\frac{\partial^2 N_{xy}}{\partial x \partial y} = \left(\frac{\partial^2 w}{\partial x \partial y}\right)^2 - \frac{\partial^2 w}{\partial x^2}\frac{\partial^2 w}{\partial y^2}, \tag{5}$$

where the membrane internal stretching forces N_x, N_y and N_{xy} are calculated from

$$N_x = \sigma_x h,\ N_y = \sigma_y h,\ N_{xy} = \tau_{xy} h. \tag{6}$$

An Euler-Lagrange analysis leads to the nonlinear ordinary differential equation describing the transverse motion expressed as [12,13]

$$\rho \frac{\partial^2 w}{\partial t^2} + c\frac{\partial w}{\partial t} - (N_x + N_{0x})\frac{\partial^2 w}{\partial x^2} - (N_y + N_{0y})\frac{\partial^2 w}{\partial y^2} - 2(N_{xy} + N_{0xy})\frac{\partial^2 w}{\partial x \partial y} = 0, \tag{7}$$

where ρ denotes aerial density of membrane, c denotes viscous damping coefficient, N_{0x} and N_{0y} denote initial tensions along axis x and y, respectively, N_{0xy} denotes initial shear force.

As the maximum transverse vibration displacement of the membrane is much smaller than the boundary size, the shearing actions among the membrane fibers are negligible [13]. In order to simplify the computation, the shearing effect will be ignored in this paper such that

$$N_{0xy} = N_{xy} = 0. \tag{8}$$

Thus, Eqs. (5) and (7) may be simplified, and we obtain the governing Euler-Lagrange partial differential equations describing free vibration problem of orthotropic membranes based on the Von Kármán's large deflection assumption:

$$\begin{cases} \rho \dfrac{\partial^2 w}{\partial t^2} + c\dfrac{\partial w}{\partial t} - (N_x + N_{0x})\dfrac{\partial^2 w}{\partial x^2} - (N_y + N_{0y})\dfrac{\partial^2 w}{\partial y^2} = 0 \\ \dfrac{1}{E_1 h}\dfrac{\partial^2 N_x}{\partial y^2} - \dfrac{\upsilon_1}{E_1 h}\dfrac{\partial^2 N_x}{\partial x^2} + \dfrac{1}{E_2 h}\dfrac{\partial^2 N_y}{\partial x^2} - \dfrac{\upsilon_2}{E_2 h}\dfrac{\partial^2 N_y}{\partial y^2} = \left(\dfrac{\partial^2 w}{\partial x \partial y}\right)^2 - \dfrac{\partial^2 w}{\partial x^2}\dfrac{\partial^2 w}{\partial y^2} \end{cases}. \tag{9a,b}$$

We introduce the Airy stress function φ

$$\begin{cases} N_x = h\dfrac{\partial^2 \varphi}{\partial y^2} \\ N_y = h\dfrac{\partial^2 \varphi}{\partial x^2} \end{cases},$$

(10a,b)

and substitute Eqs. (4) and (10) into Eq. (9); then Eqs. (9a,b) can be simplified as

$$\begin{cases} \rho\dfrac{\partial^2 w}{\partial t^2} + c\dfrac{\partial w}{\partial t} - \left(h\dfrac{\partial^2 \varphi}{\partial y^2} + N_{0x}\right)\dfrac{\partial^2 w}{\partial x^2} - \left(h\dfrac{\partial^2 \varphi}{\partial x^2} + N_{0y}\right)\dfrac{\partial^2 w}{\partial y^2} = 0 \\ \dfrac{1}{E_1}\dfrac{\partial^4 \varphi}{\partial y^4} + \dfrac{1}{E_2}\dfrac{\partial^4 \varphi}{\partial x^4} - 2\dfrac{\upsilon_1}{E_1}\dfrac{\partial^4 \varphi}{\partial x^2 \partial y^2} = \left(\dfrac{\partial^2 w}{\partial x \partial y}\right)^2 - \dfrac{\partial^2 w}{\partial x^2}\dfrac{\partial^2 w}{\partial y^2} \end{cases}. \quad (11a,b)$$

We make the following fundamental definitions to transform into non-dimensional space and time variables

$$\begin{aligned} &\bar{x} = x/a,\ \bar{y} = y/b,\ \bar{w} = w/a,\ \bar{N}_{0\bar{x}} = N_{0x}/\left(E_1 h\right),\ \bar{N}_{0\bar{y}} = N_{0y}/\left(E_1 h\right), \\ &\bar{t} = t\sqrt{E_1 h/\rho a^2},\ \bar{c} = c\sqrt{a^2/\rho E_1 h},\ \bar{\varphi} = \varphi/\left(E_1 a^2\right),\ \eta = E_1/E_2,\ \kappa = a/b, \end{aligned}, \quad (12a,b)$$

leading to the dimensionless equations

$$\begin{cases} \dfrac{\partial^2 \bar{w}}{\partial \bar{t}^2} + \bar{c}\dfrac{\partial \bar{w}}{\partial \bar{t}} - \bar{N}_{0\bar{x}}\dfrac{\partial^2 \bar{w}}{\partial \bar{x}^2} - \kappa^2 \bar{N}_{0\bar{y}}\dfrac{\partial^2 \bar{w}}{\partial \bar{y}^2} - \kappa^2 \dfrac{\partial^2 \bar{\varphi}}{\partial \bar{x}^2}\dfrac{\partial^2 \bar{w}}{\partial \bar{y}^2} - \kappa^2 \dfrac{\partial^2 \bar{\varphi}}{\partial \bar{y}^2}\dfrac{\partial^2 \bar{w}}{\partial \bar{x}^2} = 0 \\ \kappa^2 \dfrac{\partial^4 \bar{\varphi}}{\partial \bar{y}^4} + \dfrac{\eta}{\kappa^2}\dfrac{\partial^4 \bar{\varphi}}{\partial \bar{x}^4} - 2\upsilon_1 \dfrac{\partial^4 \bar{\varphi}}{\partial \bar{x}^2 \partial \bar{y}^2} = \left[\left(\dfrac{\partial^2 \bar{w}}{\partial \bar{x} \partial \bar{y}}\right)^2 - \dfrac{\partial^2 \bar{w}}{\partial \bar{x}^2}\dfrac{\partial^2 \bar{w}}{\partial \bar{y}^2}\right] \end{cases}. \quad (13a,b)$$

In this investigation, the membrane boundary conditions are assumed to be the simply supported boundary conditions expressed as

$$\begin{cases} \bar{w}(\bar{x}, \bar{y}, t) = 0 \\ \dfrac{\partial^2 \bar{w}}{\partial \bar{x}^2}(\bar{x}, \bar{y}, t) = 0 \\ \dfrac{\partial^2 \bar{w}}{\partial \bar{y}^2}(\bar{x}, \bar{y}, t) = 0 \end{cases} \quad \text{at} \quad \bar{x} = 0,1;\ \bar{y} = 0,1. \quad (14)$$

2.2 Modal Expansion. In order to apply the Galerkin method, a set of expansion functions must be chosen. The previous studies [11-16] only assumed symmetric basis functions; however, at large amplitudes, the asymmetric modes may also participate at the same order, contributing to different energy pathways through coupling to the symmetric modes. Thus, the expanded displacement variable $\bar{w}$ should include expansions of both basis function sets. The asymmetric part in the assumed vibration mode shape plays an important role, as it can have a counteracting softening effect on the frequency response [20].

Solving the nonlinear equations of membrane structure by a perturbation procedure [21], we may obtain a general solution for the transverse displacement. First, the mode shape obtained from the corresponding linearized vibration problem may be chosen as the seed mode

$$\bar{w}(\bar{x},\bar{y},\bar{t}) = \bar{W}_0(\bar{t})\sin(q\bar{x})\sin(p\bar{y}), \tag{15}$$

where $\bar{W}_0(\bar{t})$ denotes time-dependent modal function for the first-order solution, $q = m\pi/a$, $p = n\pi/b$, m and n denote the number of half-waves along x and y axis, respectively. Subsequently, we can obtain the second-order solution from the first perturbation as

$$\bar{W}_1(\bar{t})\sin(2q\bar{x}) + \bar{W}_2(\bar{t})\cos(2p\bar{y})\sin(2q\bar{x}), \tag{16}$$

where $\bar{W}_1(\bar{t})$, $\bar{W}_2(\bar{t})$ denote time-dependent modal functions for the second-order solution.

Based on the first two modal order solutions, we may identify the third-order solution as

$$\bar{W}_3(\bar{t})\sin(q\bar{x})\sin(p\bar{y}) + \bar{W}_4(\bar{t})\sin(q\bar{x})\sin(3p\bar{y}) + \bar{W}_5(\bar{t})\sin(3q\bar{x})\sin(p\bar{y}) + \bar{W}_6(\bar{t})\sin(3q\bar{x})\sin(3p\bar{y}). \tag{17}$$

where $\bar{W}_3(\bar{t}) - \bar{W}_6(\bar{t})$ denote time-dependent modal functions for the third-order solution.

From the procedure, the following general expression considering both symmetric and asymmetric modes can be summarized as

$$\bar{w}(\bar{x},\bar{y},\bar{t}) = \sum_{i=1,3,5\ldots}^{\infty}\sum_{j=1,3,5\ldots}^{\infty}\bar{W}_{ij}(\bar{t})\sin(iq\bar{x})\sin(jp\bar{y}) + \sum_{k=2,4,6\ldots}^{\infty}\sum_{l=0,2,4\ldots}^{\infty}\bar{W}_{kl}(\bar{t})\sin(kq\bar{x})\cos(lp\bar{y}), \tag{18}$$

where $\bar{W}_{ij}(\bar{t})$, $\bar{W}_{kl}(\bar{t})$ are time-dependent unknown functions.

By imposing the boundary conditions Eq. (14), the transverse displacement field from Eq. (18) can be expressed as

$$\bar{w}(\bar{x},\bar{y},\bar{t}) = \sum_{i=1,3,5\ldots}^{\infty}\sum_{j=1,3,5\ldots}^{\infty}\bar{W}_{ij}(\bar{t})\sin(iq\bar{x})\sin(jp\bar{y}) + \sum_{\alpha=2,4,6\ldots}^{\infty}\sum_{\beta=0,2,4\ldots}^{\infty}\bar{W}_{\alpha\beta}(\bar{t})\sin(\alpha q\bar{x})\left\{\frac{15+6\beta}{28+12\beta}\right. \\ \left. -\cos\left[(14+6\beta)p\bar{y}\right]+\frac{13+6\beta}{28+12\beta}\cos\left[(16+6\beta)p\bar{y}\right]\right\} \quad (19)$$

We selected and retained the first four terms that include symmetric and asymmetric coupling terms

$$\bar{w}^{*}(\bar{x},\bar{y},\bar{t}) = \bar{w}_{11}{}^{*}(\bar{x},\bar{y},\bar{t}) + \bar{w}_{20}{}^{*}(\bar{x},\bar{y},\bar{t}) + \bar{w}_{22}{}^{*}(\bar{x},\bar{y},\bar{t}) + \bar{w}_{13}{}^{*}(\bar{x},\bar{y},\bar{t}) \\ = \bar{W}_{11}(\bar{t})\sin(q\bar{x})\sin(p\bar{y}) + \bar{W}_{20}(\bar{t})\sin(2q\bar{x}) + \bar{W}_{22}(\bar{t})\sin(2q\bar{x})\left[\frac{3}{4}-\cos(2p\bar{y})+\frac{1}{4}\cos(4p\bar{y})\right] \\ +\bar{W}_{13}(\bar{t})\sin(q\bar{x})\sin(3p\bar{y}) \quad (20)$$

where $\bar{w}_{11}{}^{*} - \bar{w}_{13}{}^{*}$ are the first four mode functions varying with time and space, $\bar{W}_{11} - \bar{W}_{13}$ are the corresponding time-dependent modal amplitude functions.

The present analysis treats the vibration problem as a type of strong modal coupling, where every mode vibrates with comparable and independent amplitude [21]. These modes represent both symmetric and asymmetric components of the membrane deformation pattern. The first double series in Eq. (19) represents the flexural modes, revealing hardening features of vibration with odd multiples of the basic wave numbers i and j. The second double series in Eq. (19) represents the coupling modes including flexural and axial modes, revealing softening features of vibration with even multiples of basic wave numbers α and β [22].

Using the selected modal functions Eq. (20), we can obtain a set of governing ordinary differential equations for the modal amplitudes

$$\begin{cases} \dfrac{\partial^2 \overline{w}_{11}^{\,*}}{\partial \overline{t}^{\,2}} + \overline{c}\dfrac{\partial \overline{w}_{11}^{\,*}}{\partial \overline{t}} - \overline{N}_{0\overline{x}}\dfrac{\partial^2 \overline{w}_{11}^{\,*}}{\partial \overline{x}^{\,2}} - \kappa^2 \overline{N}_{0\overline{y}}\dfrac{\partial^2 \overline{w}_{11}^{\,*}}{\partial \overline{y}^{\,2}} - \kappa^2 \dfrac{\partial^2 \overline{\varphi}}{\partial \overline{x}^{\,2}}\dfrac{\partial^2 \overline{w}_{11}^{\,*}}{\partial \overline{y}^{\,2}} - \kappa^2 \dfrac{\partial^2 \overline{\varphi}}{\partial \overline{y}^{\,2}}\dfrac{\partial^2 \overline{w}_{11}^{\,*}}{\partial \overline{x}^{\,2}} = 0 \\ \dfrac{\partial^2 \overline{w}_{20}^{\,*}}{\partial \overline{t}^{\,2}} + \overline{c}\dfrac{\partial \overline{w}_{20}^{\,*}}{\partial \overline{t}} - \overline{N}_{0\overline{x}}\dfrac{\partial^2 \overline{w}_{20}^{\,*}}{\partial \overline{x}^{\,2}} - \kappa^2 \overline{N}_{0\overline{y}}\dfrac{\partial^2 \overline{w}_{20}^{\,*}}{\partial \overline{y}^{\,2}} - \kappa^2 \dfrac{\partial^2 \overline{\varphi}}{\partial \overline{x}^{\,2}}\dfrac{\partial^2 \overline{w}_{20}^{\,*}}{\partial \overline{y}^{\,2}} - \kappa^2 \dfrac{\partial^2 \overline{\varphi}}{\partial \overline{y}^{\,2}}\dfrac{\partial^2 \overline{w}_{20}^{\,*}}{\partial \overline{x}^{\,2}} = 0 \\ \dfrac{\partial^2 \overline{w}_{22}^{\,*}}{\partial \overline{t}^{\,2}} + \overline{c}\dfrac{\partial \overline{w}_{22}^{\,*}}{\partial \overline{t}} - \overline{N}_{0\overline{x}}\dfrac{\partial^2 \overline{w}_{22}^{\,*}}{\partial \overline{x}^{\,2}} - \kappa^2 \overline{N}_{0\overline{y}}\dfrac{\partial^2 \overline{w}_{22}^{\,*}}{\partial \overline{y}^{\,2}} - \kappa^2 \dfrac{\partial^2 \overline{\varphi}}{\partial \overline{x}^{\,2}}\dfrac{\partial^2 \overline{w}_{22}^{\,*}}{\partial \overline{y}^{\,2}} - \kappa^2 \dfrac{\partial^2 \overline{\varphi}}{\partial \overline{y}^{\,2}}\dfrac{\partial^2 \overline{w}_{22}^{\,*}}{\partial \overline{x}^{\,2}} = 0 \\ \dfrac{\partial^2 \overline{w}_{13}^{\,*}}{\partial \overline{t}^{\,2}} + \overline{c}\dfrac{\partial \overline{w}_{13}^{\,*}}{\partial \overline{t}} - \overline{N}_{0\overline{x}}\dfrac{\partial^2 \overline{w}_{13}^{\,*}}{\partial \overline{x}^{\,2}} - \kappa^2 \overline{N}_{0\overline{y}}\dfrac{\partial^2 \overline{w}_{13}^{\,*}}{\partial \overline{y}^{\,2}} - \kappa^2 \dfrac{\partial^2 \overline{\varphi}}{\partial \overline{x}^{\,2}}\dfrac{\partial^2 \overline{w}_{13}^{\,*}}{\partial \overline{y}^{\,2}} - \kappa^2 \dfrac{\partial^2 \overline{\varphi}}{\partial \overline{y}^{\,2}}\dfrac{\partial^2 \overline{w}_{13}^{\,*}}{\partial \overline{x}^{\,2}} = 0 \end{cases} . \quad (21)$$

Before the Galerkin technique is fully applied, the Airy stress function $\overline{\varphi}$ should firstly be found. Based on the structure of assumed shape function $\overline{w}^*$ and Eq. (13b), we may build the stress function as shown in Table 1.

Table 1 Assumed mode shape and corresponding stress functions

Mode order		Expression
1	$\overline{w}$	$\overline{W}_{11}(\overline{t})\sin(q\overline{x})\sin(p\overline{y})$
	$\overline{\varphi}$	$\overline{\xi}_1(\overline{t})\cos(2q\overline{x}) + \overline{\xi}_2(\overline{t})\cos(2p\overline{y})$
2	$\overline{w}$	$\overline{W}_{20}(\overline{t})\sin(2q\overline{x})$
	$\overline{\varphi}$	$\overline{\xi}_3(\overline{t})\cos(3q\overline{x})\sin(p\overline{y}) + \overline{\xi}_4(\overline{t})\sin(3q\overline{x})\sin(p\overline{y})$
3	$\overline{w}$	$\overline{W}_{22}(\overline{t})\sin(2q\overline{x})\left[\dfrac{3}{4} - \cos(2p\overline{y}) + \dfrac{1}{4}\cos(4p\overline{y})\right]$
	$\overline{\varphi}$	$\overline{\xi}_5(\overline{t})\cos(3q\overline{x})\sin(p\overline{y}) + \overline{\xi}_6(\overline{t})\sin(3q\overline{x})\sin(p\overline{y}) + \overline{\xi}_7(\overline{t})\cos(4q\overline{x}) + \overline{\xi}_8(\overline{t})\cos(4p\overline{y})$ $+\overline{\xi}_9(\overline{t})\sin(4p\overline{y}) + \overline{\xi}_{10}(\overline{t})\sin(4q\overline{x}) + \overline{\xi}_{11}(\overline{t})\sin(8p\overline{y}) + \overline{\xi}_{12}(\overline{t})\sin(8q\overline{x})$
4	$\overline{w}$	$\overline{W}_{13}(\overline{t})\sin(q\overline{x})\sin(3p\overline{y})$
	$\overline{\varphi}$	$\overline{\xi}_{13}(\overline{t})\cos(2q\overline{x}) + \overline{\xi}_{14}(\overline{t})\cos(2p\overline{y}) + \overline{\xi}_{15}(\overline{t})\cos(4p\overline{y})\sin(2q\overline{x}) + \overline{\xi}_{16}(\overline{t})\sin(4p\overline{y})\sin(2q\overline{x})$

Unlike previous studies where only symmetric modes were assumed in the mode shape functions and corresponding stress functions [11-16], the asymmetric modes are considered and added into the expansions in this work, which led to the modal coupling terms in

displacement and stress functions. It is noted that the displacement is expanded by linear modal functions in displacement coordinates in this paper, unlike the nonlinear normal modes (NNM) method, where a pair of state variables (displacement and velocity) are chosen as master coordinates to solve the nonlinear problem [23, 24].

Upon substituting the expressions for $\bar{\varphi}$ and $\bar{w}$ into Eq. (13b), the time-dependent unknown functions $\bar{\xi}_i(\bar{t})$ may be obtained. Then, we may apply the Galerkin method to transform the partial differential equations (PDEs) to a system of ordinary differential equations (ODEs) by discretization of the space variables. Consequently, the following system of nonlinear differential equations is obtained

$$\begin{cases} \dfrac{\mathrm{d}^2\bar{W}_{11}}{\mathrm{d}\bar{t}^2} + d_1\dfrac{\mathrm{d}\bar{W}_{11}}{\mathrm{d}\bar{t}} + d_2\bar{W}_{11} + \bar{W}_{11}\left(r_1\bar{W}_{11}^2 + r_2\bar{W}_{11}\bar{W}_{20} + r_3\bar{W}_{11}\bar{W}_{22} + r_4\bar{W}_{11}\bar{W}_{13} + r_5\bar{W}_{20}\bar{W}_{22} + r_6\bar{W}_{20}\bar{W}_{13} + r_7\bar{W}_{22}\bar{W}_{13}\right) = 0 \\ \dfrac{\mathrm{d}^2\bar{W}_{20}}{\mathrm{d}\bar{t}^2} + d_3\dfrac{\mathrm{d}\bar{W}_{20}}{\mathrm{d}\bar{t}} + d_4\bar{W}_{20} + \bar{W}_{20}\left(r_1\bar{W}_{11}^2 + r_2\bar{W}_{11}\bar{W}_{20} + r_3\bar{W}_{11}\bar{W}_{22} + r_4\bar{W}_{11}\bar{W}_{13} + r_5\bar{W}_{20}\bar{W}_{22} + r_6\bar{W}_{20}\bar{W}_{13} + r_7\bar{W}_{22}\bar{W}_{13}\right) = 0 \\ \dfrac{\mathrm{d}^2\bar{W}_{22}}{\mathrm{d}\bar{t}^2} + d_5\dfrac{\mathrm{d}\bar{W}_{22}}{\mathrm{d}\bar{t}} + d_6\bar{W}_{22} + \bar{W}_{22}\left(r_1\bar{W}_{11}^2 + r_2\bar{W}_{11}\bar{W}_{20} + r_3\bar{W}_{11}\bar{W}_{22} + r_4\bar{W}_{11}\bar{W}_{13} + r_5\bar{W}_{20}\bar{W}_{22} + r_6\bar{W}_{20}\bar{W}_{13} + r_7\bar{W}_{22}\bar{W}_{13}\right) = 0 \\ \dfrac{\mathrm{d}^2\bar{W}_{13}}{\mathrm{d}\bar{t}^2} + d_7\dfrac{\mathrm{d}\bar{W}_{13}}{\mathrm{d}\bar{t}} + d_8\bar{W}_{13} + \bar{W}_{13}\left(r_1\bar{W}_{11}^2 + r_2\bar{W}_{11}\bar{W}_{20} + r_3\bar{W}_{11}\bar{W}_{22} + r_4\bar{W}_{11}\bar{W}_{13} + r_5\bar{W}_{20}\bar{W}_{22} + r_6\bar{W}_{20}\bar{W}_{13} + r_7\bar{W}_{22}\bar{W}_{13}\right) = 0 \end{cases}, \quad (22)$$

where the coefficients d_i modify the linear terms and the coefficients r_i modify the nonlinear terms. We can see the presence of cubic nonlinearities in the modal amplitudes, arising from the stretching of the median surface due to large deformation. The coupling appears in these cubic terms, which may reveal qualitative differences in nonlinear characteristics. The obtained ODEs Eq. (22) are integrated numerically by means of the fourth-order Runge-Kutta method. Consequently, some parametric relationships such as amplitude-frequency, displacement-period, mode shapes evolution, etc., may be found.

3 Experimental Validations

We conducted our experiments with a tension-ejection apparatus developed previously [14]. Fig. 2 reveals a picture of the experimental setup based on the steel bracket with two-dimensional size of 2500 mm×2500 mm. Two brands (ZZF and XYD) of membrane material were selected and made into rectangular specimens with size of 1200 mm×1200 mm. Material data is shown in Table 2. In the tension component of the apparatus, the pretension force is provided by the screw rod and translated by the clamp into the membrane surface. Then, the membrane structure can be formed and studied further with four different levels of pretension force, 1.0, 2.0, 3.0 and 4.0 kN in this study. For the ejection component, the ejection force is generated by an air pump and a pressurized plenum cylinder, both of which are computer-controlled.

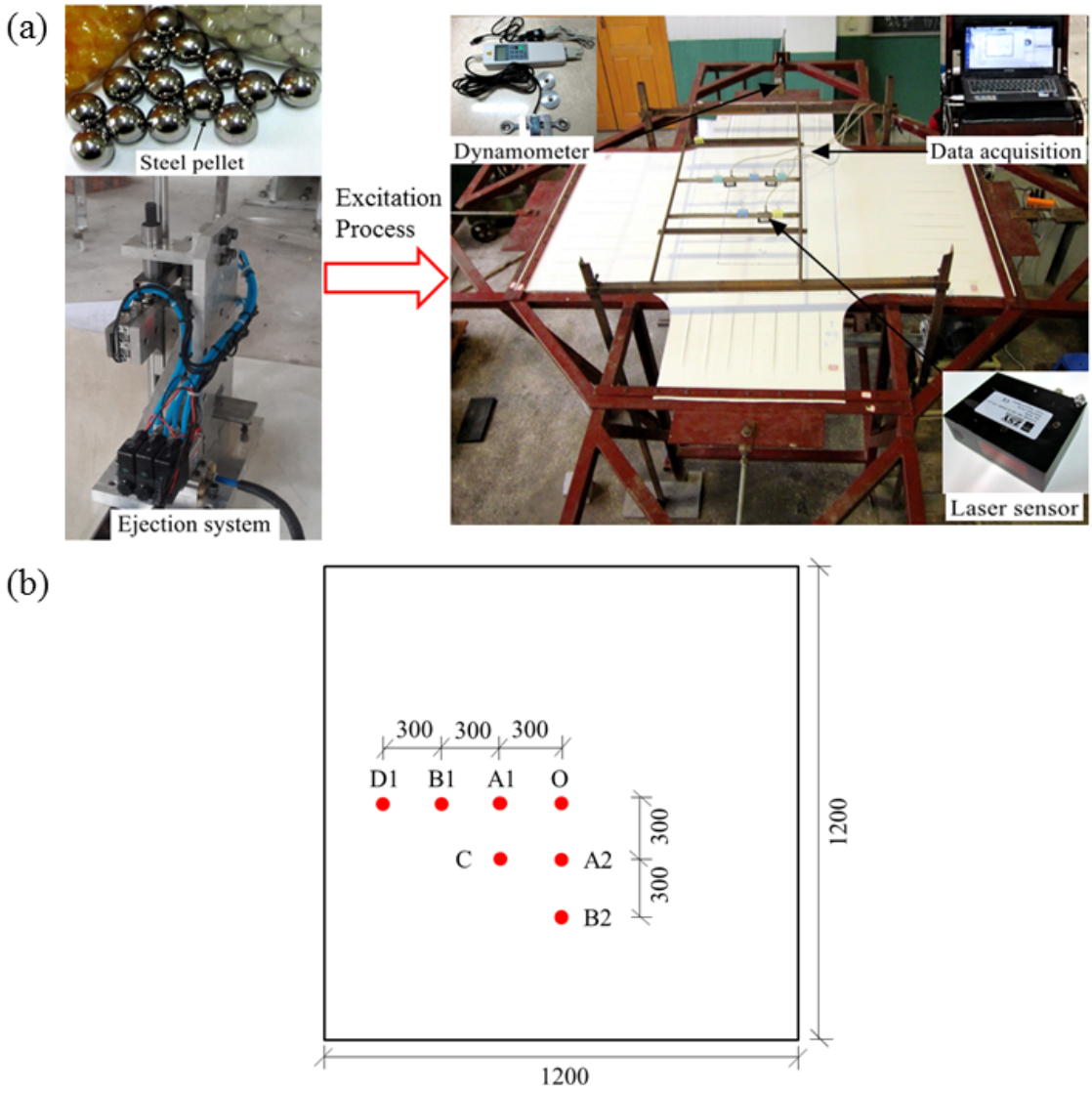

Fig. 2 Mechanical experiment. (a) Photo of experiment. (b) Distribution of measured points on membrane surface.

Initially, the membrane structure was pre-stressed with tension system providing the horizontal loads. Then, the ejection system provided the power to eject the steel pellet. Consequently, the pellet is fired at the center of the membrane $(\bar{x}_0, \bar{y}_0) = (0.5, 0.5)$ to provide an effective initial velocity through the impulse-momentum transfer from the pellet; the subsequent free vibration is then realized and studied in detail. Different effective initial

conditions may be obtained by adjusting cylinder pressure (and thus pellet velocity). Since the resulting membrane transverse vibration amplitudes typically greatly exceeded the membrane's thickness, the vibration retains substantial nonlinearity.

Table 2 Membrane material constants

Type	Density (g/m^2)	Thickness (mm)	Poisson ratio (warp/weft)	Elastic modulus (warp/weft) (Mpa)	Tensile strength (warp/weft) (N/cm)
ZZF	950	0.8	0.3/0.4	1590/1360	4300/4000/5
XYD	950	0.8	0.3/0.4	1720/1490	4400/4200/5

During the experiment, the three key parameters of pretension, initial amplitude, and displacement must be measured. For pretension measurement, a HP-10K dynamometer (with calibration range 0.01-10 kN) between clamp and screw rod was used. A laser displacement system with a 100 mm range and 2 kHz sampling rate was used to obtain amplitude data (such as the six marked dots shown in Fig. 2). The laser sensor includes RS485 serial output, trigger input, AL logic control terminal, and 5 m telemetry cable; more details on the experimental procedure are provided in Liu et al. [13].

4 Results and Discussion

4.1 Frequency Response Curves. Fig. 3 presents the amplitude-frequency relationship. The frequency Ω is normalized with respect to the first order frequency ω_{11} obtained from linear analysis. The amplitude is normalized with respect to the thickness h of membrane. Better convergent agreement is achieved when the expansion is improved with three or four modes. The model reveals the expected hardening nonlinear behavior when using only symmetric mode terms. Conversely, the asymmetric mode terms (mode order from 2 to 4) are

introduced and added in this work, which induces a softening nonlinear behavior. Furthermore, this softening behavior is validated by the available experimental data. These results are qualitatively similar to the earlier results [20,21]. It was found through trial and that error that the lowest-mode expansion able to predict the softening behavior with acceptable accuracy is 4 modes. Therefore, in the following the order-4 modal expansion will be used due to the balance of accuracy with reasonable computational effort. Clearly, the added asymmetric modes affect the nonlinear coupling, resulting in a different type of nonlinear behavior.

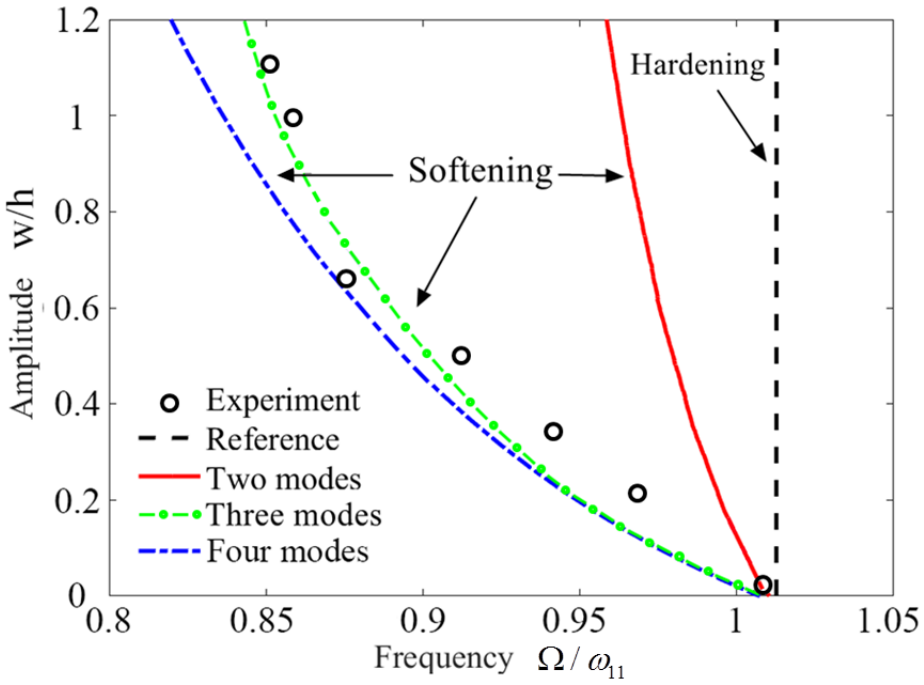

Fig. 3 Dimensionless amplitude w/h versus dimensionless first order frequency Ω/ω_{11}. The circular points represent experimental results abstracted from displacement-time signals. The dashed lines are predictions based on assumed stress functions with different modal orders.

4.2 Displacement-Time/Space Response Curves. In order to validate the model, the comparisons with experiment are conducted at the load case of 1 kN. The associated

parameters include the displacement time histories, mode shapes, and the amplitude-frequency relationship. Fig. 4 plots the experimental and theoretical curves of the displacement varying with time at Point O and B1. The small discrepancy relating to the amplitudes of oscillation occurs partly from uncertainties in the precise initial condition and noise in our experiments. Both results are decaying oscillations (as would be expected) with well-matched frequencies. It should be noted that the displacement-time curves show the asymmetric influences. From the specific dots marked as A(A')-D(D'), the value at Point B(B') is larger than that at Point A(A') with the existence of damping, and the phenomenon appears between Point D(D') and C(C') as well, which suggests the dynamic response contains asymmetric characteristics. The asymmetric response is different from the results in previous study [11,12], which may be contributed by the introduction of asymmetric assumed modes and consideration of coupled effects.

Due to the symmetry in the structure and in location of the given initial amplitude, Fig. 5 shows the vibration shape at $\bar{t} = 0$ along the x direction on a quarter of the membrane surface; theory and experiment match quite well again to within the same uncertainties and noise described above. The initial maximum amplitude affects the deflection pattern due to the nonlinearity.

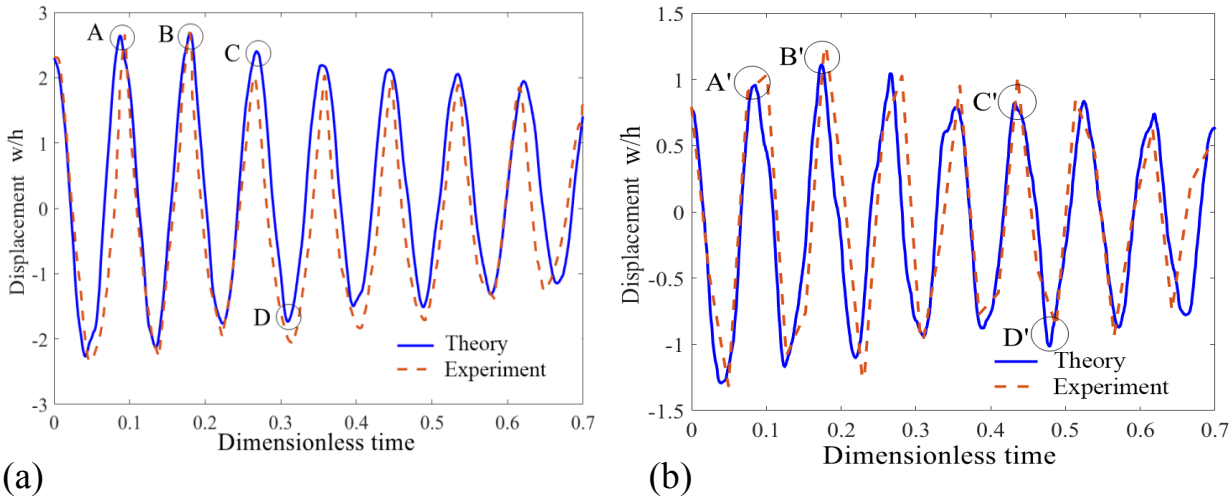

Fig. 4 Dimensionless displacement w/h versus dimensionless time $\bar{t}$. (a) Point O. (b) Point B1. The membrane material is XYD brand, and initial displacement $\bar{w}_0$ is 2.1. The solid lines represent measured data in experiment. The dashed lines are the corresponding theoretical prediction.

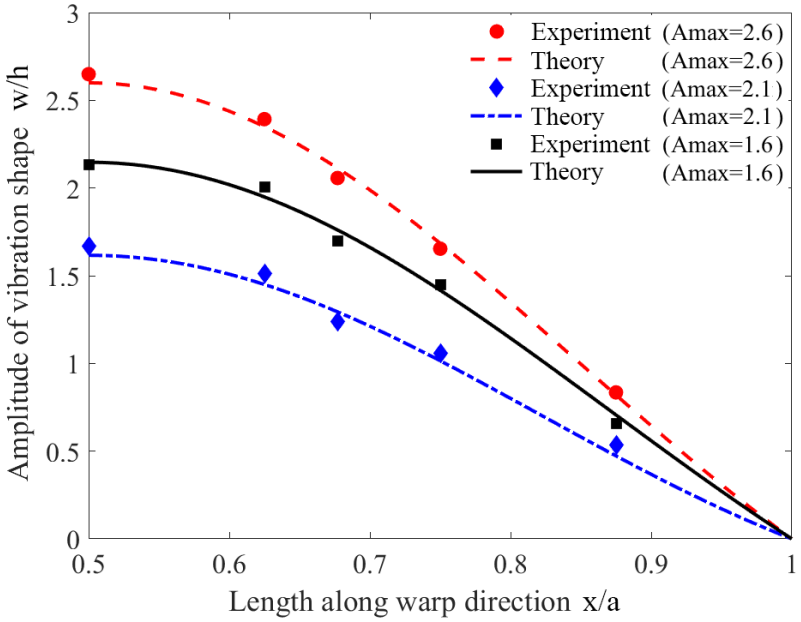

Fig. 5 Dimensionless amplitude w/h versus dimensionless coordinate position x/a on a one-quarter membrane surface at $\bar{t}=0$. The scattered points represent measured data along the weft direction in experiment. The continuous lines are predictions from theory.

4.3 Mode Shapes and Their Evolutions. Fig. 6 compares an interesting feature of the mode shapes based on the analysis with modal coupling (solid lines) and without modal coupling (dashed lines). It may be found that the amplitude-dependent mode shapes after the consideration of modal coupling would reveal more non-symmetric, spatially-localized characteristics. These differences demonstrate clearly that the coupling of symmetric and asymmetric modes will quantitatively affect the final result, particularly if performing system identification for model updating or using the modes as features for identifying structural changes (i.e., due to damage). The mode shapes vary continuously with time as well. This time-varying nature of the mode shapes is illustrated in Fig. 7, where the first two modes are represented at three different instants of time, selected during the first quarter-period of motion. It is clear that the coupling affects when symmetric vs. asymmetric effects are dominant during a cycle compared to a symmetric-only analysis.

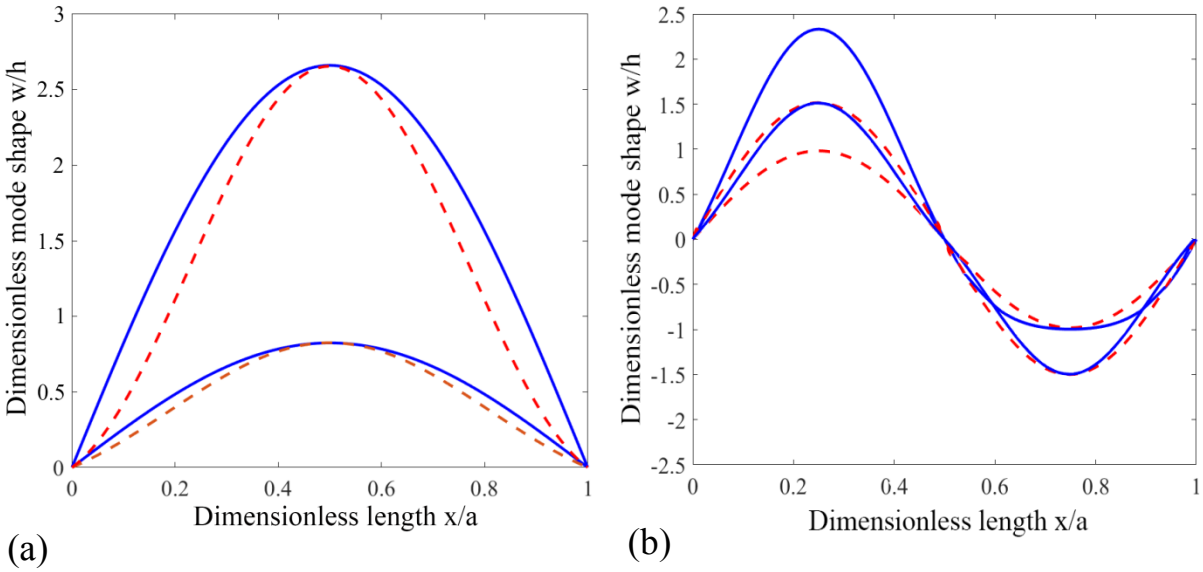

Fig. 6 Mode shapes with different initial amplitude. (a) The first order mode shape. (b) The second order mode shape. The solid lines represent the mode shape based on the analysis

including modal coupling. The dashed lines represent the mode shape based on the analysis without modal coupling.

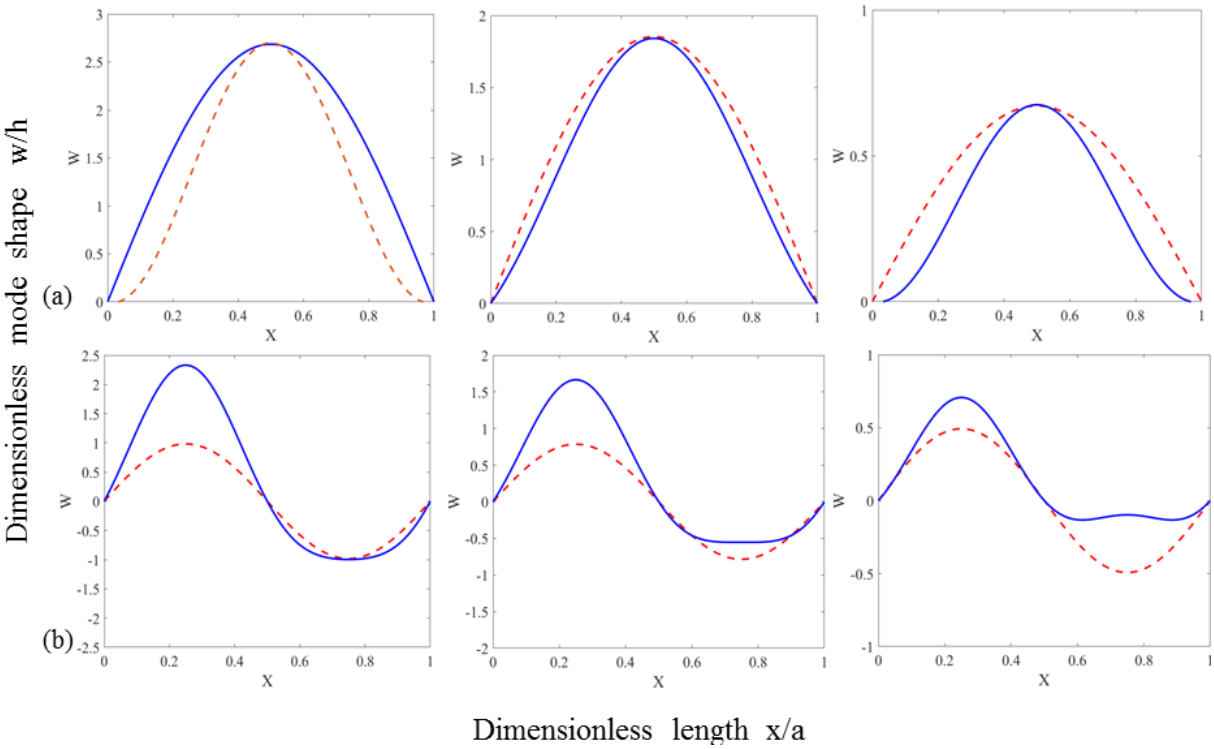

Fig. 7 Evolution of the mode shapes throughout a quarter-period of transverse motion. (a) Evolution of the first order mode shape. (b) Evolution of the second order mode shape.

4.4 Parametric Analysis. In Table 3 the experimental and theoretical normalized results of first four natural frequencies with respect to the lowest experimental frequency are tabulated and compared. It should be noted that the theoretical value is calculated based on the assumption of four mode functions. It was found that theoretical natural frequencies are fairly well correlated to the experimental values, but consistently lower, with increasing deviation with modal order. This arises from both the specific properties of the modal functions as well as the truncation order (4). For each order case, the frequency enlarges almost linearly with

increasing pretension force, which corroborates previous theoretical results derived by Liu et al. [12].

Table 3 First four frequencies with pretension force

F/F0	ω_1/ω_{11}			ω_2/ω_{11}			ω_3/ω_{11}			ω_4/ω_{11}		
	Exp.	Theory	Error (%)	Exp.	Theory	Error (%)	Exp.	Theory	Error (%)	Exp.	Theory	Error (%)
1	1.00	0.99	-1	2.69	2.66	-1.11	2.81	2.67	-1.78	3.81	3.75	-1.57
2	1.28	1.24	-1.56	3.49	3.45	-1.15	3.61	3.47	-1.66	4.94	4.98	0.81
3	1.52	1.48	-1.97	4.16	4.21	1.21	4.27	4.23	-1.41	5.84	5.75	-1.54
4	1.74	1.75	0.57	4.70	4.67	-0.64	4.88	4.69	-2.25	6.63	6.57	-0.90

Fig. 8 shows the trend of the amplitude-frequency relationship. The predicted frequencies reduce as amplitude increases varying from 2 to 8 on average. This is again the result of the softening nonlinearity, which is dominated by asymmetric mode terms. In contrast to the softening behavior, the trend transitions to a hardening-type nonlinearity stage when the amplitude exceeds 8. Here, the symmetric modes begin to dominate the response. Fig. 8 shows the effect of thickness of membrane material on the amplitude/frequency relationship; three cases of increasing thickness levels of 0.8 mm, 1.0 mm and 1.2 mm are considered. It is evident that thinner material demonstrates stronger nonlinearity in both softening and hardening stages. Moreover, thinner membrane structures transition into the hardening stage more slowly. This phenomenon is likely because the thinner membrane structure has a smaller stiffness, which will result in the stronger nonlinear vibration.

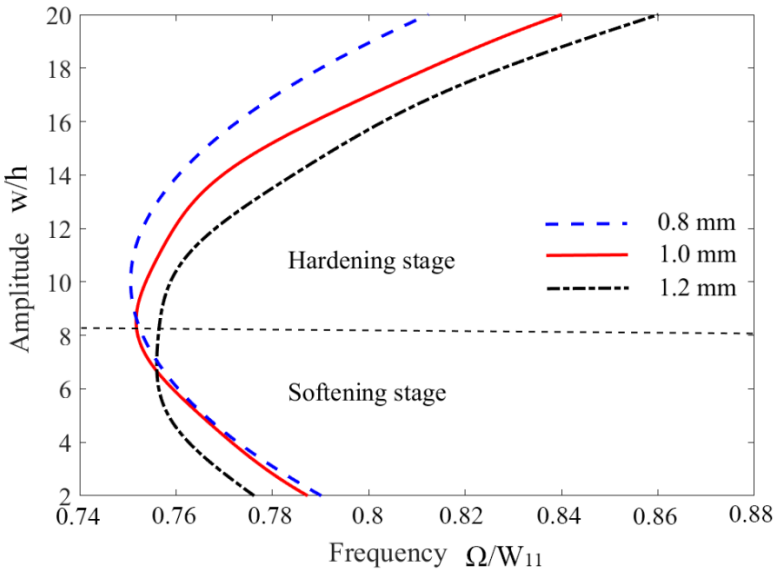

Fig. 8 Dimensionless amplitude w/h versus dimensionless first order frequency Ω/w_{11}, for different values of membrane material thickness (h=0.8mm, 1.0mm, 1.2mm).

Fig. 9 presents the first order frequency of membrane structure for various aspect ratios κ. There is a non-proportional trend in the frequency-pretension relationship with aspect ratio, particularly for larger pretension ratios from about 2 to 4; the slope changes much more significantly with higher aspect ratios, implying that the stiffness of membrane structure can be largely well-controlled with aspect ratio in conjunction with pretension.

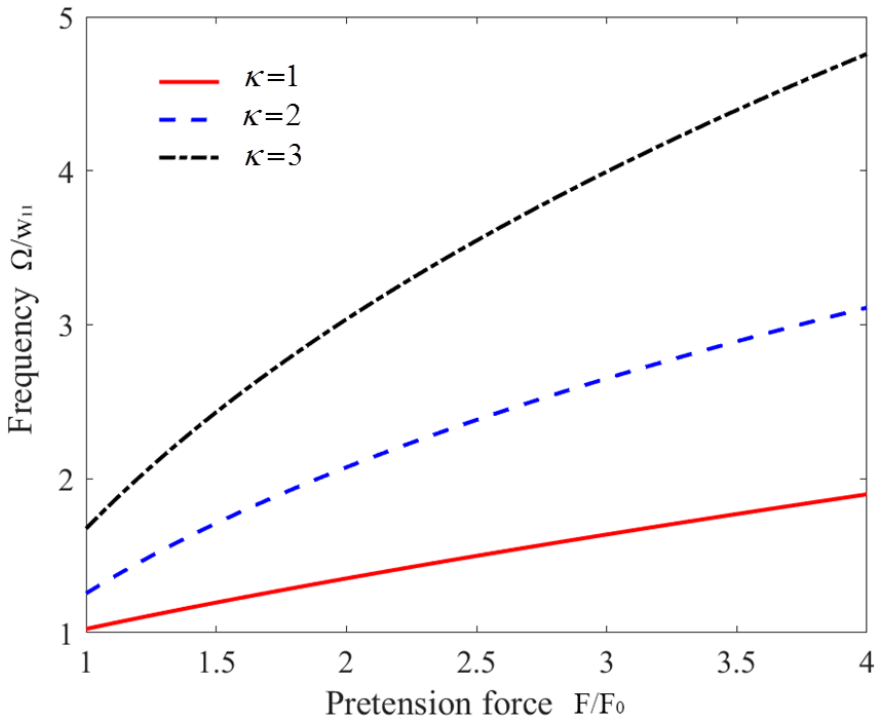

Fig. 9 Dimensionless first order frequency Ω / w_{11} versus dimensionless pretension force F / F_0 with different values of membrane aspect ratio (κ=1, 2, 3).

As the majority of membrane materials applied in engineering fields possess orthotropic characteristics due to the manufacturing progress, the properties towards the perpendicular direction (warp and weft) will be different, which has been expressed in the previously-mentioned theoretical derivation. Theoretically, the orthotropic material properties can affect the dynamic response of membrane structures. Fig. 10 shows that experiment and theory again agreed very reasonably. In order to compare the difference at characteristic points, the amplitude at Point A1 along weft direction was defined as the reference value; and the reduction rate was computed by comparing the results at other positions with the reference value under the same condition. After calculation and comparison, we can find that for the points A1 and B1 lined perpendicularly, the gap appears to be about 10% on average until

pretension force level of 2. From the range from 2-4, the gap becomes more and more limited below 5% on average. A similar trend exists at Point C, while the only difference between Point B1 and C is the greater amplitude reduction for Point C. This is dominated by the distance effect, since Point C to Point O is farther than Point B1 to Point O.

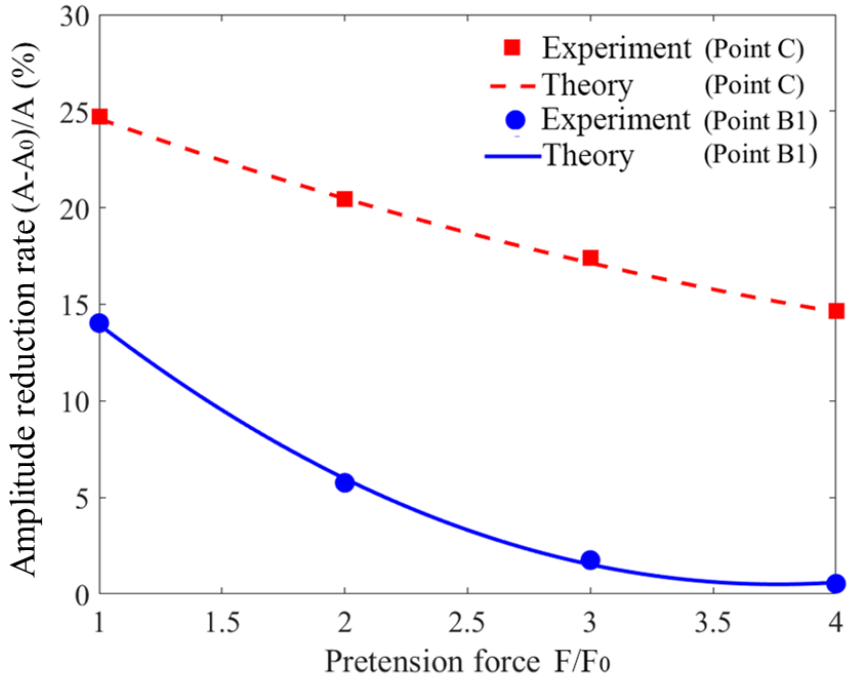

Fig. 10 Amplitude reduction rate $\left(A-A_0\right)/A$, versus dimensionless pretension force F/F_0.

5 Summary and Conclusions

In this paper, the nonlinear vibrations of orthotropic pre-tensioned membrane structures were analyzed, focusing on the coupling effect between symmetric and asymmetric modes. A combined Galerkin-numerical technique applied to von Kármán's theory led to a theoretical model that was found to be in generally good agreement with experimental results. Primary conclusions drawn from the obtained results are as follows:

(a) Unlike the purely hardening characteristics predicted in previous work, the amplitude-frequency curves obtained based on coupled effects indicated that membrane structure contains softening characteristics. Moreover, as the vibration amplitude increased, the

transition of from softening to hardening behavior was observed. These results prove that the influences of the coupling between symmetric and asymmetric modes are quite significant to predict the correct trend in frequency-amplitude relationships, at least qualitatively. This asymmetric-symmetric interaction was observed in other results, such as displacement time histories and mode shapes.

(b) The effects of thickness and aspect ratio on the nonlinear response was analyzed in detail. The nonlinearity is more observable in thinner material, and the frequency dependence upon aspect ratio increases substantially with increasing aspect ratio. The displacement dependence upon orthotropic specificity is varied within the limit of 10%.

(c) The normalized pretention force F / F_0 plays a crucial role in the nonlinear response. With larger pretention force, the frequency increases almost linearly but the displacement reduces.

The application of the present model, including modal coupling, could be extended to study other non-linear features, particularly concerning the behavior of the membrane dynamic stresses, at large amplitudes. It is desirable to predict the membrane structural failure based on the future development of membrane dynamic stress in combination with failure criterion.

Acknowledgements

The authors would like to acknowledge the following resources for funding this work:

- Natural Science Foundation of China (No. 51178485, No. 51608060)
- Fund of China Scholarship Council (No. 201706050050)

References

[1] Chadha, M., and Todd, M. D., 2017, "A Generalized Approach for Reconstructing the Three-Dimensional Shape of Slender Structures including the Effects of Curvature, Shear, Torsion, and Elongation," ASME J. Appl. Mech., **84**(4), p. 041003.

[2] Kumar, N., and DasGupta, A., 2017, "On the Static and Dynamic Contact Problem of an Inflated Spherical Viscoelastic Membrane," ASME J. Appl. Mech., **82**(12), pp. 1-8.

[3] Liu, C. J., Deng, X. W., and Zheng, Z. L., 2017, "Nonlinear Wind-induced Aerodynamic Stability of Orthotropic Saddle Membrane Structures," J. Wind Eng. Ind. Aerod., **164**, pp. 119-127.

[4] Hu, Y, Chen, W. J., Chen, Y. F., Zhang, D. X., and Qiu, Z. Y., 2017, "Modal Behaviors and Influencing Factors Analysis of Inflated Membrane Structures," Eng. Struct., **132**, pp. 413-427.

[5] Kang, S. W., and Lee, J. M., 2002, "Free Vibration Analysis of Composite Rectangular Membranes with an Oblique Interface," J. Sound Vib., **251**(3), pp. 505-517.

[6] Houmat, A., 2004, "Free Vibration Analysis of Membranes Using the *h-p* Version of the Finite Element Method," J. Sound Vib., **282**(1-2), pp. 401-410.

[7] Wu, W. X., Shu, C., and Wang C. M., 2007, "Vibration Analysis of Arbitrarily Shaped Membranes Using Local Radial Basis of Function-based Differential Quadrature Method," J. Sound Vib., **306**(1-2), pp. 252-270.

[8] Amore, P., 2008, "A New Method for Studying the Vibration of Non-homogeneous Membranes," J. Sound Vib., **321**(1-2), pp. 104-114.

[9] Noga, S., 2010, “Free Transverse Vibration Analysis of an Elastically Connected Annular and Circular Double-membrane Compound System,” J. Sound Vib., **329**(9), pp. 1507-1522.

[10] Soares, M. R., and Goncalves, P. B., 2014, “Large-amplitude Nonlinear Vibrations of a Mooney- Rivlin Rectangular Membrane,” J. Sound Vib., **333**(13), pp. 2920-2935.

[11] Zheng, Z. L., Liu, C. J., He, X. T., and Chen, S. L., 2009, “Free Vibration Analysis of Rectangular Orthotropic Membranes in Large Deflection,” Math. Prol. Eng., **2009**, pp. 1-9.

[12] Liu, C. J., Zheng, Z. L., Long, J., Guo, J. J., and Wu, K., 2013, “Dynamic Analysis for Nonlinear Vibration of Prestressed Orthotropic Membranes with Viscous Damping”, Int. J. Struct. Stab. Dy., 13(2), pp. 1350018.

[13] Liu, C. J., Todd, M. D., Zheng, Z. L., and Wu, Y. Y., 2018, “A Nondestructive Method for the Pretension Detection in Membrane Structures based on Nonlinear Vibration Response to Impact,” Struct. Health Monit., **17**(1), pp. 67-79.

[14] Guo, J. J., Zheng, Z. L., and Wu, S., 2015, “An Impact Vibration Experimental Research on the Pretension Rectangular Membrane Structure”, Adv. Mater. Sci. Eng., 2015(4), pp. 1-8.

[15] Zheng, Z. L., Lu, F. M., He, X. T., Sun, J.Y., Xie, C. X., and He, C., 2016, “Large Displacement Analysis of Rectangular Orthotropic Membranes under Stochastic Impact Loading”, Int. J. Struct. Stab. Dy., 16(1), pp. 1640007.

[16] Li, D., Zheng, Z. L., Liu, C. Y., Zhang, G. X., Lian, Y. S., Tian, Y., Xiao, Y., Xie, and X. M., 2017, "Dynamic Response of Rectangular Prestressed Membrane Subjected to Uniform Impact Load," Arch. Civ. Mech. Eng., **17**(3), pp. 586-598.

[17] Laura, P. A. A., Bambill, D. V., and Gutierrez, R. H., 1997, "A Note on Transverse Vibration of Circular , Annular, Composite Membranes," J. Sound Vib., **205**(5), pp. 692-697.

[18] Touze, C., Thomas, O., and Huberdeau, A., 2004, "Asymptotic Non-linear Normal Modes for Large-amplitude Vibrations of Continuous Structures," Comput. Struct., **82**, pp. 2671-2682.

[19] Lau, S., and Cheung, Y. K., 2009, "Amplitude Incremental Variational Principle for Nonlinear Vibration of Elastic Systems," ASME J. Appl. Mech., **48**(4), pp. 959-964.

[20] Goncalves, P. B., and Del Prado, Z. J. G. N., 2002, "Nonlinear Oscillations and Stability of Parametrically Excited Cylindrical Shells," Meccanica, **37**(6), pp. 569-597.

[21] Goncalves, P. B., Silva, F. M. A., and Del Prado, Z. J. G. N., 2008, "Low-Dimensional Models for the Nonlinear Vibration Analysis of Cylindrical Shells based on a Perturbation Procedure and Proper Orthogonal Decomposition," J. Sound Vib., **315**, pp. 641-663.

[22] Lazarus, A., Thomas, O., and De ü , J. F., 2012, "Finite Element Reduced Order Models for Nonlinear Vibrations of Piezoelectric Layered Beams with Applications to NEMS," Finite Elem. Anal. Des., 49, pp. 35-51.

[23] Pesheck, E., Pierre, C., and Shaw, S. W., 2002, "Modal Reduction of a Nonlinear Rotating Beam through Nonlinear Normal Modes", J. Vib. Acoust., 124, pp. 229-236.

[24] Kerschen, G., Peeters, M., Golinval, J. C., and Vakakis, A. F., 2009, “Nonlinear Normal Modes, Part I: A Useful Framework for the Structural Dynamicist”, Mech. Syst. Signal Pr., 23, pp. 170-194.